Available online at www.sciencedirect.com

ScienceDirect

Procedia CIRP 133 (2025) 14–19

www.elsevier.com/locate/procedia

20th CIRP Conference on Modeling of Machining Operations

Modeling Process Forces in CFRP Grinding: Influence of Cutting Materials and Coolant on Process Force Behavior

Alexander Brouschkin[a]*, Carsten Möller[a], Jan Hendrik Dege[a]

[a]*Institute of Production Management and Technology, Hamburg University of Technology, Denickestr. 17, 21073 Hamburg*
* Corresponding author. Tel.: +49 42878 3264; E-*mail address:* alexander.brouschkin@tuhh.de

Abstract

Carbon Fibre Reinforced Polymer (CFRP) is favoured for its high strength to weight ratio, excellent directional mechanical and thermal properties, and the ability to be optimized in the direction of stress or heat flow. These properties make it ideal for power transmission applications. Meeting the high-quality requirements in this area requires a precise grinding process and a thorough understanding of cutting forces, which are influenced by different factors e.g. coolant usage, or cutting material. However, machining unidirectional CFRP is challenging due to its anisotropic behaviour, resulting in different machining forces for identical parameters with different fibre orientations.
A universal process-independent model was recently developed to describe the engagement conditions during oblique cutting of unidirectional CFRP by introducing the spatial fibre cutting angle θ_0 and the spatial engagement angle φ_0.Using this description, an universal mechanistic machining force model for grinding of CFRP was developed.
In the paper, an extension of the model of oblique cutting for grinding is extended and experimentally verified, taking into account additional parameters e.g. coolant and cutting material. Therefore, the process forces were measured as a function of the spatial fibre cutting angles for different cutting materials, both with and without the use of coolant.

Peer-review under responsibility of the scientific committee of the 20th CIRP Conference on Modeling of Machining Operations in Mons

Keywords: CFRP, grinding, process forces, modeling, spatial engagement conditions

1. Introduction

Carbon fibre reinforced polymers (CFRP) are used for their excellent weight specific mechanical properties. CFRP consists of carbon fibres and a polymer matrix. The fibres exhibit anisotropic behaviour and are responsible for transferring mechanical and thermal loads in the composite. The polymer matrix supports the fibres against lateral loads, distributes the load between the fibres and protects the fibres from environmental influences.

In order to comply with tolerance requirements, FRP components often have to be machined on contours, surfaces or holes at the end of the manufacturing process chain [1]. Tools with geometrically defined cutting edges, such as end mills [2] and drills [3], are used for contouring and drilling respectively. Grinding tools with geometrically indeterminate cutting edges are used both for surface machining and for contour machining of component contours [4].

To comply with tolerance requirements, reliably design, monitor and optimise machining processes, knowledge of the machining force is very important. In addition to the measurement of machining forces, model-based force prediction also plays an important role. Mechanistic force models, which calculate the force based on force coefficients and corresponding chip sizes, are widely used for defined cutting edges [2, 3] and grinding [5, 6, 7]. Since the force coefficients are determined experimentally as a function of the material being machined, the engagement conditions and the cutting parameters, these are empirical or semi-empirical models. The force coefficients of continuous fibre reinforced polymers are largely determined by the orthotropic structure of the material. When machining CFRP, this results in a

2212-8271
Peer-review under responsibility of the scientific committee of the 20th CIRP Conference on Modeling of Machining Operations in Mons
10.1016/j.procir.2025.02.004

characteristic machining behaviour that depends on the kinematics of the machining action relative to the longitudinal direction of the fibre. Wang distinguishes between different separation mechanisms when milling CFRP, which also occur when machining CFRP and are already known from wood machining [7, 8]. Accordingly, the fibre cutting angle θ, which is defined as the included angle between the local cutting direction of the tool in the engagement area and the longitudinal direction of the fibre, is decisive for the separation mechanism.

Karpat et al. [2] and Boudelier et al. [7] developed a mechanistic force model for predicting machining forces in milling and grinding operations respectively for CFRP using a trigonometric function to model the impact of fibre orientation and a linear dependency of the forces on the uncut chip thickness h [2].

Nomenclature

CFRP	Carbon fibre reinforced polymer
Cor.	Corundum
Dia.	Diamond
Cool.	Usage of coolant
$\overrightarrow{e_{\|\|}}, \overrightarrow{e_{\perp 1}}, \overrightarrow{e_{\perp 2}}$	Coordinate system of the CFRP laminate
$\overrightarrow{e_r}, \overrightarrow{e_s}, \overrightarrow{e_o}$	Coordinate system of the cutting tool
$\overrightarrow{e_t}, \overrightarrow{e_k}, \overrightarrow{e_n}$	Local coordinate system of the cutting tool segment
$\vec{p}$	Position vector for tool segments
θ	Fibre cutting angel [°]
χ, ξ	Reference angles [°]
θ_0	Spatial fibre cutting angle [°]
φ_0	Spatial fibre engagement angle [°]
ρ	Grinding wheel inclination angle [°]
$\vec{F}$	Force [N]
t	Index: Tangential
n	Index: Normal
c	Index Seperation
e	Index: Friction
F_n	Normal force [N]
v_c	Cutting speed [m/s]
f	Feed rate [mm/rev]
n	Spindle speed [rpm]
a_p	depth of cut [mm]
b	Width of undeformed chip [mm]
h	Undeformed chip thickness [mm]
t_b, b_b, l_f	Dimensions of the CFRP block [mm]
D	Grinding wheel diameter [mm]
b	Grinding wheel width [mm]
Gr	Grit size [mesh]
G	Grain size [µm]
S	Structure of the grinding wheel
ϕ	Engagement angle [°]
N	Number of cutting edges
K_c	Cutting force coefficient [N/mm²]
K_e	Friction force coefficient [N/mm]
m_c	Exponent of specific cutting force
K^*	Modelled force Coefficient

Köttner et al. [9] developed a machining force model that takes into account the three-dimensional engagement conditions on the fibre, which are defined by the spatial fibre cutting angle θ_0 and the fibre engagement angle φ_0. It is a mechanistic approach by Lee and Altintas, which is mainly used for machining with a defined cutting edge [10]. As with Arslan and Budak, it is extended to include a friction component [5].

This work extends and modifies the model established by Köttner et al. to a wider feed range, conventional cutting materials such as corundum and the use of cooling. To this end, systematic experiments are carried out with corundum and diamond tools. The new applications result in a non-linear dependency of the griding forces on the feed which has not been observed so far for CFRP. Therefore, an adapted cutting force model is developed and validated.

2. Process-independent description of fibre engagement conditios

A process-independent description of the spatial engagement conditions during the oblique cut of CFRP with reference angles, in which they applied a transformation of the workpiece coordinate system $\{\overrightarrow{e_{||}}, \overrightarrow{e_{\perp 1}}, \overrightarrow{e_{\perp 2}}\}$ into the tool coordinate system $\{\overrightarrow{e_r}, \overrightarrow{e_s}, \overrightarrow{e_o}\}$ (Figure 1) was developed by Hintze et al.[11]. With the reference angles θ, χ, ξ and the inclination angle λ_s any cutting process can be described. Considering the orthotropy of CFRP, Hintze et al. [11] introduce the spatial engagement angles, which describe the spatial angles between the vectors $\overrightarrow{e_s}$ and $\overrightarrow{e_{||}}$ for the spatial fibre cutting angle θ_0 and between the vectors $\overrightarrow{e_r}$ and $\overrightarrow{e_{||}}$ for the spatial engagement angle φ_0, as shown in Figure 1 a). With the equations (1-3) θ_0 and φ_0 can be calculated.

$$\begin{pmatrix} \overrightarrow{e_{||}} \\ \overrightarrow{e_{\perp 1}} \\ \overrightarrow{e_{\perp 2}} \end{pmatrix} = \begin{bmatrix} \cos\theta & \sin\theta & 0 \\ -\sin\theta & \cos\theta & 0 \\ 0 & 0 & 1 \end{bmatrix} \cdot \begin{bmatrix} 1 & 0 & 0 \\ 0 & \cos\chi & \sin\chi \\ 0 & -\sin\chi & \cos\chi \end{bmatrix} \cdot \begin{bmatrix} \cos\xi & 0 & -\sin\xi \\ 0 & 1 & 0 \\ \sin\xi & 0 & \cos\xi \end{bmatrix} \cdot \begin{pmatrix} \overrightarrow{e_r} \\ \overrightarrow{e_s} \\ \overrightarrow{e_o} \end{pmatrix} \quad (1)$$

$$\cos(\theta_0) = \langle \overrightarrow{e_r}, \overrightarrow{e_{||}} \rangle \quad (2)$$

$$\cos(\varphi_0) = \langle \overrightarrow{e_s}, \overrightarrow{e_{||}} \rangle \quad (3)$$

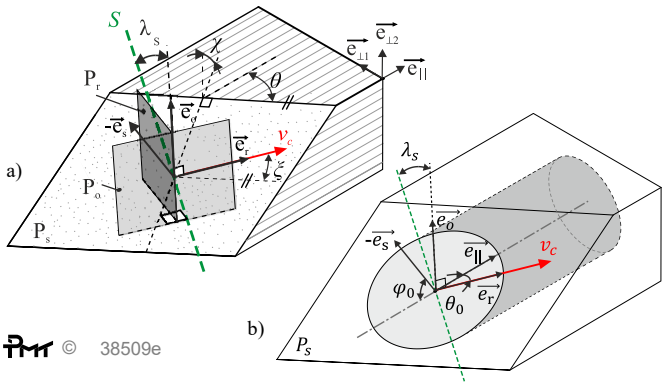

Figure 1: a) Workpiece coordinate system and the tool coordinate system with the reference angles, b) spatial engagement angles

3. Experimental Setup

The experiments are carried out using the experimental set-up shown in Figure 2. A unidirectional CFRP specimen (HexPly 6367, HTS-(12K)) is clamped to a dynamometer (Kistler 9257B). Grinding wheels with an outer diameter of D = 200 mm and a width of b = 20 mm are used. Two different

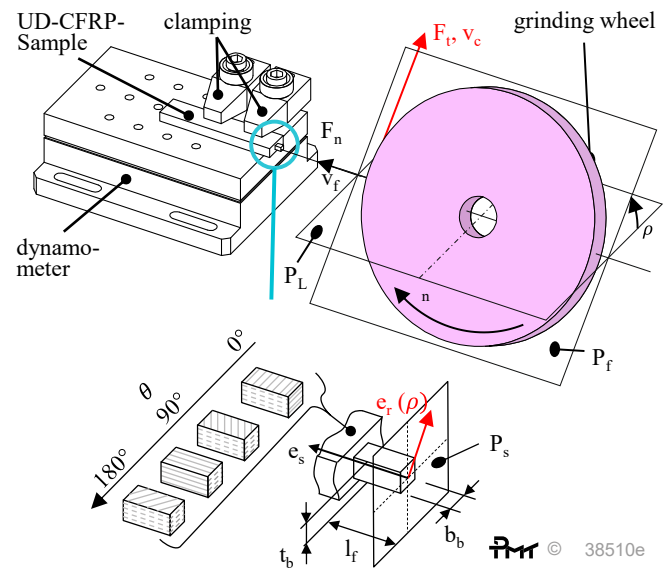

Figure 2: Experimental setup

cutting materials are used: Corundum with a ceramic bond, a grit size of Gr = 46 mesh (G = 301 µm) and a structure of S = 11, and single-layer electroplated diamond with a grain size of G = 301 µm. The use of coolant and dry machining are also investigated. Blaser B-Cool 675 emulsion, approx. 8% is used as coolant. The experiments are carried out at a cutting speed v_c = 10 m/s, which corresponds to a rotational speed n = 955 rpm. The feed rate f = 0.05|0.15|0.3|0.6 mm/rev is also varied.

In a machining operation prior to the examination, a block with the dimensions t_b = 3.6 mm, b_b = 3.6 mm and l_f = 2.5 mm is cut free at the tip of the sample in order to avoid interference with the disc face during the main examination. The square cross-sectional area is always aligned parallel to the feed direction. Different spatial engagement conditions are realised by varying the fibre cutting angle θ and the grinding wheel inclination angle ρ (Table 1), with the tool rotation axis in the centre plane of the specimen. As a result of the large disc diameter and the low material thickness, the engagement angle can be assumed to be $\phi \approx 90°$ over the entire engagement range. The following applies to the calculation of the spatial engagement conditions:

$$\chi = 0° ; \xi = \rho \quad (4)$$

$$\theta_0 = \arccos[\cos(\theta) \cdot \cos(\xi)] \quad (5)$$

$$\varphi_0 = \arccos[\sin(\theta)] \quad (6)$$

Regarding equations (7) and (8) $\rho = 0° \ldots 90°$ and $\theta = 0° \ldots 180°$ is sufficient to cover all possible engagement conditions. The position of the measurement points in the θ_0,φ_0-plane is shown in (Figure 3). Part of the measurements are used to build the model and part are used to validate the model. The distribution between model and validation tests is shown in Table 1.

The measured force signals are low-pass filtered with a cut-off frequency of 10 Hz, averaged over the engagement time and, after offset correction, converted by coordinate transformation into grinding normal force F_n and grinding tangential force F_t.

Table 1: Parameter for variation of spatial engagement conditions

Tilt ρ [°]	Fiber cutting angle θ [°]	Type
0	0, 15, 30, 45, 60, 75, 90, 105, 120, 135, 150, 165	Model building
30	0, 15, 30, 45, 135, 150, 165	Validation
45	0, 15, 30, 45, 135, 150, 165	Validation
60	0, 15, 30, 45, 60, 120, 135, 150, 165	Model building
90	0, 15, 30, 45, 60, 75, 90	Model building

4. Force measurements results

Figure 4a shows the measurement results for the tangential and normal forces at feed rates f = 0.05 mm/rev and f = 0.6 mm/rev for corundum with cooling in the θ_0,φ_0-plane. The results are shown as contour plots in the definition area of the spatial engagement conditions θ_0,φ_0, which form a triangle. At low feed rates the maximum forces occur at $\theta_0 = 90°$ and $\varphi_0 = 45° \ldots 60°$. From there the forces decrease almost concentrically. The drop to decreasing θ_0 is greater than to increasing θ_0 . As a result, the tangential forces at f = 0.05 mm/rev are approximately symmetrical to the line $\theta_0 = 90°$. At feed f = 0.6 mm/rev, the maximum tangential forces occur in the range $90° < \theta_0 < 135°$ and $0° < \varphi_0 < 45°$, while the minimum tangential forces occur in the range $30° < \theta_0 < 60°$ and $30° < \varphi_0 < 60°$. A similar qualitative distribution of forces has been reported with other CFRP-material and cutting material combinations for grinding [9] and for machining with

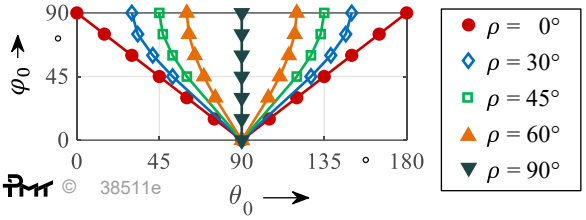

Figure 3: Measurements in θ_0-φ_0-plane

a defined cutting edge [12]. The minimum of the forces is explained by the occurrence of compressive stresses and thus induced interlaminar fractures [9, 12]. For normal forces, the minimum forces occur in the same range as for tangential forces. In the range $90° < \theta_0 < 135°$ and $0° < \varphi_0 < 45°$, high forces occur in the same area as for the tangential forces, with the maximum forces occurring around the point $\theta_0 = 0°$ and $\varphi_0 = 90°$. This can be explained by the clogging of the chip spaces, as the largest chips are observed at $\theta = 0°$ [13]. Furthermore, the tangential forces are significantly lower than the normal forces. Assuming that the tangential forces correlate with the cutting forces and the normal forces with the feed forces when cutting with a defined cutting edge, this has been reported [12, 13].

In general, a change in the qualitative cutting behaviour of the CFRP can be observed with increasing feed rates for grinding with corundum and coolant. This shift causes a non-linear dependence of the cutting forces to the uncut chip thickness h respectively the feed f under certain engagement conditions, which can be seen in Figure 4b. In the case of dry machining and diamond cutting material in general, this change

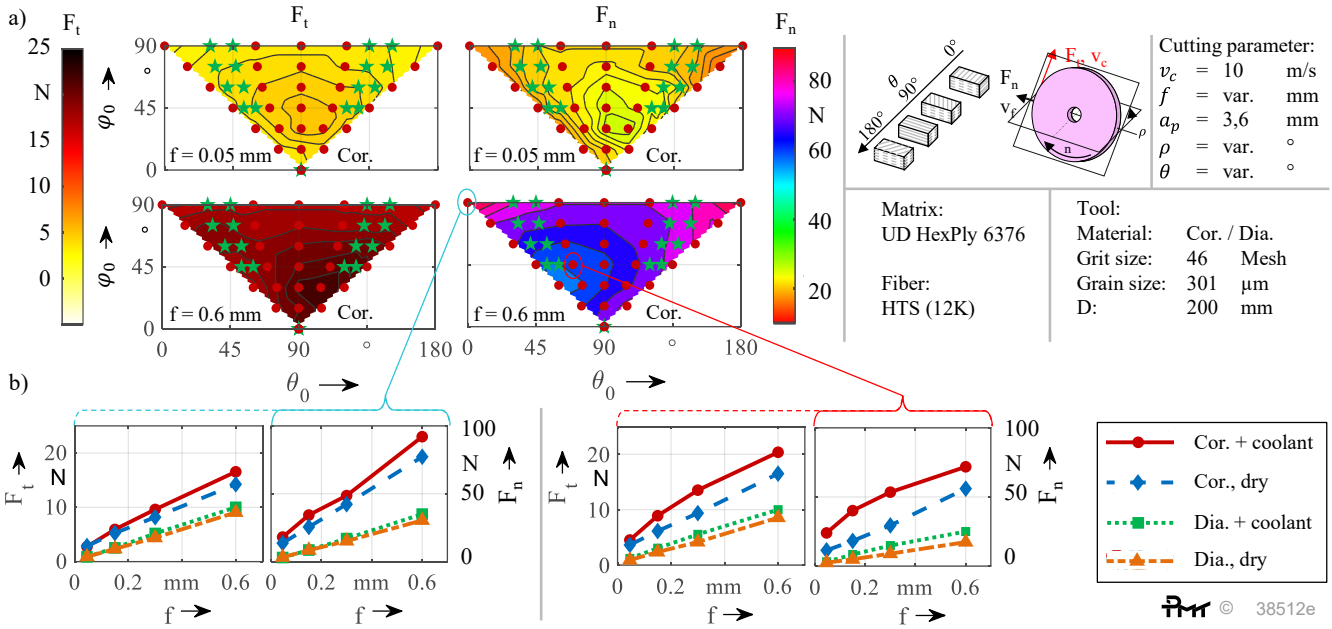

Figure 4: a) Force measurements in the θ_0-φ_0-plane, b) Forces in dependence of the feed rate

does not occur and the cutting forces show a linear dependence on the feed rate. This non-linear shift for certain spatial engagement conditions can be explained by the occurrence of compressive stresses and thus induced interlaminar fractures. Hereby, it can be concluded that machining with coolant results in low temperature which leads to higher matrix strength, making the CFRP less susceptible to interlaminar fracture. This is illustrated by the propagation of minimum forces to larger θ_0 as feed rates increase. Han et al. have shown that higher penetration depths of a cutting edge favour large area damage, probably caused by inter-fibre fractures [14].

Köttner et al. [9] described a model for predicting cutting forces when the cutting force is linearly dependent on the feed rate. This paper therefore extends Köttners's model to include the non-linear dependence of cutting forces on feed rate.

5. Mechanistic force model

The total force results from the elementary force components dF_t and dF_n transformed into the tool coordinate system in the tangential and normal directions, which are integrated for all cutting edge elements N in the engagement area:

$$\vec{F} = \sum_{i=1}^{N_i} \int_{\phi_e}^{\phi_a} [e_t \; e_n] \cdot \begin{bmatrix} dF_t \\ dF_n \end{bmatrix} \tag{7}$$

To simulate the forces, Köttner et al. use a model by Arslan and Budak [5], which has been transferred to grinding with the integration of a frictional force component. For the case of corundum with coolant, this is supplemented by an exponential dependence of the cutting forces on the uncut chip thickness based on Kienzle. The constant m_c is determined for a stable model, while the cutting force coefficient $\overrightarrow{K_c} = (K_{ct} \; K_{cn})^T$ and the friction force coefficient $\overrightarrow{K_e} = (K_{et} \; K_{en})^T$ take into account the material-specific cutting mechanisms due to the dependence on the spatial engagement conditions θ_0, φ_0.

$$\begin{bmatrix} dF_t \\ dF_n \end{bmatrix} = \begin{bmatrix} K_{et} \\ K_{en} \end{bmatrix} \cdot db \cdot r \cdot d\phi + \begin{bmatrix} K_{ct} \\ K_{cn} \end{bmatrix} \cdot db \cdot dh^{1-m_c} \tag{8}$$

5.1. Contact zone model

Analogue to Köttner et al. [9], for each cutting edge segment a position vector $\overrightarrow{p_i}$ and a local coordinate system $\{\overrightarrow{e_t}, \overrightarrow{e_k}, \overrightarrow{e_n}\}$ is defined. $\overrightarrow{e_k}$ is the direction of the cutting tool contour, $\overrightarrow{e_n}$ is the local vector normal to the machined surface and $\overrightarrow{e_t}$ is the local vector in the direction of the cutting velocity. Thus, the geometric engagement parameters of the tool are determined. The uncut machining parameter are defined as follows:

$$db = |\overrightarrow{p_{i+1}} - \overrightarrow{p_i}| \tag{9}$$

$$dh = \frac{f}{2\pi} \cdot \langle \overrightarrow{e_n}, \overrightarrow{e_f} \rangle \cdot d\phi \tag{10}$$

Angle of entry ϕ_e and exit ϕ_a remain as in Köttner et al. [9].

5.2. Force coefficients

The measurements (model building: Table 1) are used to determine the separation and friction coefficients of the mechanistic force model. Equations 7 and 8 are used to do this. Assuming that the engagement conditions are approximately constant during the tests, $\int d\phi = \Delta\phi$ can be simplified.

$$\begin{bmatrix} F_t \\ F_n \end{bmatrix} = \begin{bmatrix} K_{et} \\ K_{en} \end{bmatrix} \cdot \frac{\Delta\phi \cdot D}{2} \cdot b_b + \begin{bmatrix} K_{ct} \\ K_{cn} \end{bmatrix} \cdot b_b \cdot \left(f \cdot \frac{\Delta\phi}{2\pi} \right)^{1-m_c} \tag{11}$$

To determine the constant exponent of specific cutting force m_c, a linear regression of the model support points is performed according to equation 11. The exponent mc is increased in steps of 0,1. The mc with the highest overall coefficient of determination R^2 is selected. For corundum with coolant, this gives $m_c = 0.2$. In the other cases there is a linear relationship $m_c = 0$. The force coefficients are then calculated for the model points.

Figure 5 shows the cutting force coefficients for the tangential and normal forces for all the machining variations investigated. Corundum with coolant leads to normal cutting

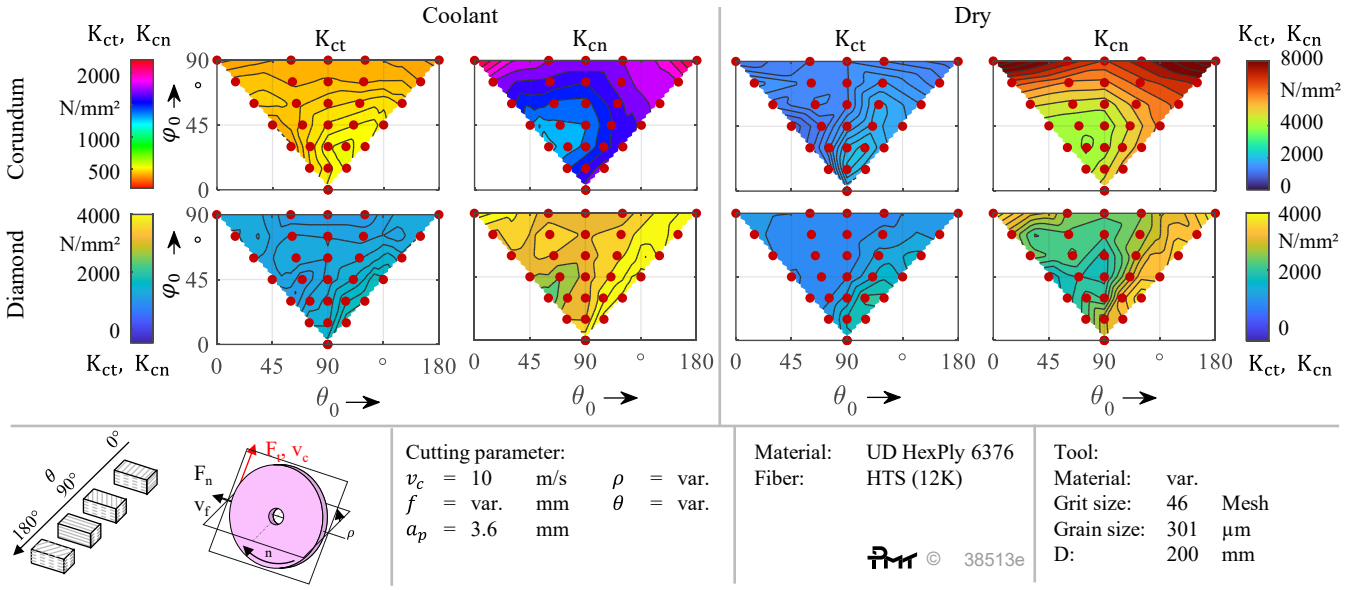

Figure 5: Experimental force coefficients K_{cn} and K_{ct}

force coefficients to vary between K_{cn} = 1000 … 2500 N/mm² and between K_{ct} = 400 … 550 N/mm² for the tangential force.

Whereas, corundum with dry machining and m_c = 0 leads to K_{cn} = 4000 … 8000 N/mm² and between K_{ct} = 1400 … 2200 N/mm². For diamond, K_{cn} varies between 2000 and 4500 N/mm² and K_{ct} between 1000 and 2000 N/mm². The minima of the cutting force coefficients occur in the range $30° < \theta_0 < 60°$ and $30° < \varphi_0 < 60°$. While the maximum cutting force coefficients for corundum occur around $\theta_0 = 0°$ and $\varphi_0 = 90°$, these are $90° < \theta_0 < 180°$ and $\varphi_0 = \theta_0$-90° for diamond in a strip. The general dependence of the force coefficients in the θ_0-φ_0-plane are same as for the machining forces and can be explained with the change of separation mechanisms. Furthermore, the forces with coolant are higher than during dry machining which can be attributed to higher temperatures during dry machining and therefore lesser stiffness of the CFRP. The large difference between the different cutting materials is probably due to the different hardness of the cutting materials, so that the forces are significantly lower for diamond than for corundum. The friction coefficient $\overrightarrow{K_e}$ behaves qualitatively similar to the cutting coefficient $\overrightarrow{K_c}$, but its value is very low and represent only 0.2% of the force value, therefore is not shown.

5.3. Modeling force coefficients

Köttner et al. [9] describe two separation mechanisms, k_1 and k_2, for modelling the force coefficients. k_1 describes the separation mechanism with dominant compressive loads in the fibre direction, favouring interlaminar fractures formation and interfibre fractures.

$$k_1(\theta_0, \varphi_0) = a_1 - a_2 \cdot \cos(2\varphi_0 - 2\theta_0) \quad (12)$$

The influence of the varying number of severed fibres with changing spatial fibre engagement angle φ_0 is described by k_2:

$$k_2(\varphi_0) = a_1 + a_2 \cdot \cos(2\varphi_0 - a_3) \quad (13)$$

The force coefficients are therefore:

$$K^*(\theta_0, \varphi_0) = a_1 \cdot (a_2 - \cos(2\theta_0 - 2\varphi_0)) \cdot (a_3 + \cos(2\varphi_0 - a_4)) + a_0 \quad (14)$$

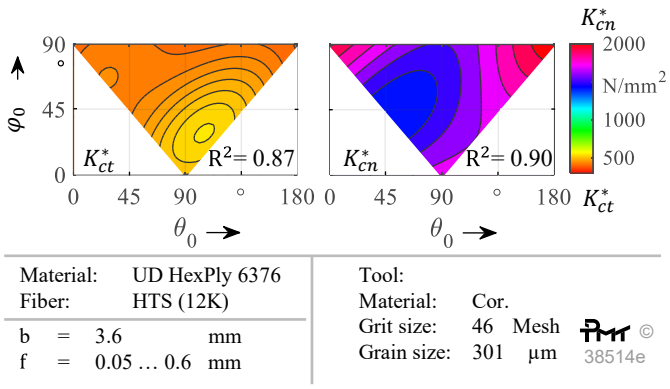

Figure 6: Modelled force coefficients

Table 2: Model parameter for the force coefficients

	a_0	a_1	a_2	a_3	a_4	Process
Unit	N/mm²	N/mm²	-	-	°	
K^*_{ct}	466.8	52.93	0.796	0.046	52	Cor. cool.
K^*_{et}	-0.67	0.0017	-38.73	12.81	78	
K^*_{cn}	532	24.96	11.72	7.72	52	
K^*_{en}	1.87	0.451	0.96	-0.645	52	
K^*_{ct}	1713	202.5	0.46	0.0864	64	Cor., dry
K^*_{et}	0.263	0.085	0.54	0.86	30	
K^*_{cn}	3720	277.3	-9.26	-4.04	52	
K^*_{en}	0.876	0.303	0.619	1.26	150	
K^*_{ct}	1286	142.7	0.497	0.982	32	Dia. cool.
K^*_{et}	0.049	0.022	0.905	0.047	54	
K^*_{cn}	4342	1111	-0.964	1.392	137	
K^*_{en}	0.140	0.078	0.212	-0.244	57	
K^*_{ct}	1041	214.6	0.638	0.959	44	Dia., dry
K^*_{et}	0.049	0.022	0.905	0.047	54	
K^*_{cn}	2571	1.981	-101.3	142.1	0	
K^*_{en}	0.185	0.074	0.429	0.447	42	

To determine the model parameters (a_0-a_6), the model is fitted to experimentally determined force coefficients using non-linear regression. The method of least squares for non-linear functions is used. The corresponding minimisation

problem was solved using the Trust-Region algorithm in Matlab. The model parameters are given in Table 2 and the corresponding functional values of the modelled release force coefficients are shown in Figure 6 as examples for the normal and tangential force components K_{cn}^{*} and K_{ct}^{*} for corundum with coolant.

6. Validation

Figure 7 shows the correlation between the modelled and measured forces Ft and Fn for measurement points not used in the model for machining with corundum and coolant. The relative error ΔF_n = 6.9 % and ΔF_t = 5.6 % show no significant differences between the measured and modelled forces.

The model is also capable of predicting the linear dependence of cutting forces on feed rate with small deviations, as is case for machining with diamond and dry machining with corundum as was shown by Köttner et al. [9].

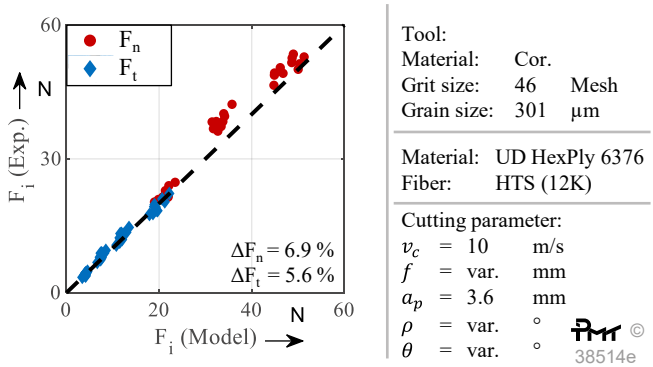

Figure 7: Correlation of the modelled and measured forces

7. Summary and Outlook

In describing the spatial conditions for grinding CFRP, the following statements can be summarised with regard to the use of different cutting materials, cooling variants and force modelling:

- The cutting material corundum produces significantly higher cutting forces than diamond, which can be attributed to the different hardness of the cutting material.
- Cooling results in slightly higher forces than dry machining. This is due to the higher machining temperature and therefore lower stiffness of the CFRP.
- The machining forces for corundum with cooling are not linearly dependent on the feed rate. This is due to the increasing influence of interlaminar cracks in the CFRP as the feed rate increases.
- The presented model is capable of predicting machining forces of different spatial engagement conditions in the CFRP.
- In the future, it is planned to transfer the model to other grinding processes such as cylindrical grinding and to integrate it into a deformation and removal model.
- There appears to be an interaction between the cutting material and the use of coolant as the combination of corundum and coolant results in a significantly different force behavior as other investigated combinations. Future work will focus on modelling this interaction by measuring the cutting temperature of dry and wet machining.

Acknowledgements

The authors gratefully acknowledge the financial support of the Federal Ministry for Economic Affairs and Climate (Bundesministerium für Wirtschaft und Klimaschutz, BMWK) within the research project SPOTLIGHT, project number 03LB2061.

References

[1] Ozkan, D.; Gok, M. S. und Karaoglanli, A. C., 2020, Carbon fiber reinforced polymer (CFRP) composite materials, their characteristic properties, industrial application areas and their machinability. Engineering Design Applications III: Structures, Materials and Processes: S. 235–253, doi: 10.1007/978-3-030-39062-4_20

[2] Karpat Y., Onur B., Deger B., 2012, Mechanistic force modeling for milling of unidirectional carbon fiber reinforced polymer laminates, International Journal of Machine Tools & Manufacture 56 (2012) 79–93, doi:10.1016/j.ijmachtools.2012.01.001

[3] Wang Q.,Jia X., Hu B., Xia W., 2019, A mechanistic prediction model of instantaneous cutting forces in drilling of carbon fiber-reinforced polymer, The International Journal of Advanced Manufacturing Technology (2019) 103:1977–1988, doi: 1 0.1007/s00170-019-03571-y

[4] Soo, S. L., Shyha, I. S., Barnett, T., Aspinwall, D. K., Sim, W.-M., 2012, Grinding performance and workpiece integrity when superabrasive edge routing carbon fibre reinforced plastic (CFRP) composites. CIRP Annals, 61, 1, S. 295–298., doi: 10.1016/j.cirp.2012.03.042

[5] Brinksmeier, E., Aurich, J. C., Govekar, E., Heinzel, C., Hoffmeister, H.-W., Klocke, F., Peters, J., Rentsch, R., Stephenson, D. J., Uhlmann, E., Weinert, K., Wittmann, M., 2006, Advances in Modeling and Simulation of Grinding Processes. CIRP Annals, 55, 2, S. 667–696, doi:10.1016/j.cirp.2006.10.003

[6] Aslan, D., Budak, E., 2014, Semi-analytical Force Model for Grinding Operations. Procedia CIRP, 14, S. 7–12, doi:/10.1016/ j.procir.2014.03.073

[7] Boudelier, A., Ritou, M., Garnier, S., Furet, B., 2018,Cutting force model for machining of CFRP laminatewith diamond abrasivecutter. Production Engineering,12,2, S.279–287., doi:10.1007/s11740-018-0813-4

[8] Wang DH., Ramulu M., Arola D., 1995, Orthogonal cutting mechanisms of graphite/epoxy composite. Part I: Unidirectional laminate. Int. Journal of Machine Tools & Manufacture, 35, 12, S. 1623-1638

[9] Köttner, L.,Jakele, L., Hintze, W., 2024, Kraftmodellierung beim Schleifen von UD-CFK unter räumlichen Eingriffsbedingungen. Schweizer Schleif-Symposium, doi:10.15480/882.13314

[10] Lee, P., Altintas, Y., 1996, Prediction of ball-end milling forces from orthogonal cutting data. International Journal of Machine Tools and Manufacture, 36, 9, S. 1059–1072, doi:10.1016/0890-6955(95)00081-X

[11] Hintze, W.; Brouschkin, A.; Köttner, L.; Bluehm, M., 2022, Model Based Prediction of Force and Roughness Extrema Inherent in Machining of Fibre Reinforced Plastics Using Data Merging. Proceedings of the 12th Congress of the German Academic Association for Production Technology (WGP), University of Stuttgart, October 2022, Springer Verlag Berlin, doi:10.1007/978-3-031-18318-8_5

[12] Brouschkin, A., Hintze, W., Dege, J.H., 2024, Influence of spatial engagement angles on machining forces and surface roughness in turning of unidirectional CFRP. CIRP journal of manufacturing science and technology 51: 201-212, doi:10.15480/882.9602

[13] Lopresto V., Santo L., Caprino G., De Iorio I., 2001, Mechanisms of chip generation in orthogonal machining of unidirectional carbon fibre reinforced plastics. Proceedings PRIME, Sestri Levante, Italy, 20.-22. Juni, 2001, S. 81-86

[14] Han, L.; Zhang, J.; Liu, Y.; Sun, T., 2021, Effect of Fiber Orientation on Depth Sensing Intralaminar Failure of Unidirectional CFRP Under Nano-Scratching. Composites Part B: Engineering 224, 109211, doi:10.1016/j.compositesb.2021.109211